Metrol. Meas. Syst., Vol. 25 (2018) No. 1, pp. 203–211.

PAN POLSKA AKADEMIA NAUK

METROLOGY AND MEASUREMENT SYSTEMS

Index 330930, ISSN 0860-8229

www.metrology.pg.gda.pl

M&MS

METROLOGICAL ASPECTS OF EVALUATION OF GLASS TYPES USED IN PHOTOVOLTAIC MODULES IN LABORATORY SCALE

Zbigniew M. Starowicz, Kazimierz Drabczyk, Katarzyna Gawlińska, Paweł Zięba

Institute of Metallurgy and Materials Science of the Polish Academy of Sciences, 25 Reymonta, 30-059, Cracow, Poland (✉ *zbigniew.starowicz@gmail.com*, +48 12 295 2863, *kazimierz.drabczyk@wp.pl*, *katarzynagawlinska@wp.pl*, *p.zieba@imim.pl*)

Abstract

The front glass cover is the crucial part of commercially available silicon solar modules as it provides mechanical protection and environmental isolation. However, from a utility point of view the most important thing is how the glass cover influences the power generation of a photovoltaic (PV) module. Optical matching of the whole structure determines the number of photons absorbed by the solar cells and hence the produced photocurrent. In this study five types of PV glass were optically measured and characterized to find out useful information on transmittance and its character. Then, the results were compared with the electrical parameters of solar mini-modules employing each type of glass. Additionally, the work aimed to providing a low-cost measuring procedure to determine the influence of front glass on photovoltaic performance in small, laboratory scale preserving the Standard Test Conditions. An important aspect was an analysis of different types of glass texture. To confirm properness and adequacy of the analysis, the uncertainty aspect was discussed as well.

Keywords: photovoltaics, silicon solar cells, module glass cover, lamination process.

1. Introduction

Photovoltaics (PV) is one of the leading technologies in the field of renewable energy sources. This is reflected by the number of 300 GW_p of the worldwide power capacity surpassed in 2016 [1] and the previous year's increment of the order of 30% [1]. This increase corresponds to the total capacity at the end of 2011. Such common interest and application is a result of high stability and reliability of PV modules. Especially, the technology of crystalline silicon solar cells is widely used, with a share in the market exceeding 90% – as indicated in the Photovoltaic Report from Fraunhofer Insititute [2]. The reason why Si modules are so robust, are good cell stability and a well-developed encapsulation process [3–6]. A standard PV module consists of a back-sheet, an encapsulant, a silicon cell, a second encapsulant and a front glass cover. Tedlar–Poliester–Tedlar (TPT) back-sheet is mostly used, while the most common encapsulant is EVA foil – copolymer of ethylene and vinyl acetate. During the lamination process at an elevated temperature of ca. 150°C the EVA foil is crosslinked and chemically bonded to the glass through the hydroxyl and silanol bonding [7] which makes the module hermetic and durable. Besides

Article history: received on Aug. 28, 2017; accepted on Oct. 14, 2017; available online on Mar. 26, 2018, DOI: 10.24425/118161.

the good lamination properties, the front glass cover should provide the mechanical resistance and – which is the most important – should be characterized by a high transmittance and optical fit to the cells. A typical glass for photovoltaic modules is a 3–4 mm thick tampered glass with a reduced content of iron oxides. Its surface can be either flat or textured in a different fashion in nano-, through micro- and millimetre scale. Although for a textured glass a decrease of optical loss is predicted due to the light trapping effect [8] (especially at a steeper angle), its outdoor performance appears to be worse due to the increased accumulation of dust and dirt [9,10]. Research is underway on a self-cleaning casing that enables to maintain improved optical properties [9]. A suitable alternative is also the use of anti-reflective coating, avoiding in this way an undesired extension of the glass surface [10–12].

While a great effort has been put into developing the technology of solar cells, much less attention in the literature was paid to encapsulation processes, and only a few papers considered the photovoltaic types of glass. Furthermore, no clear testing procedure of optical match of the PV module parameters was presented for differently structured glass. Usually, besides the measured total transmittance, the glass types are not well described since it is hard to predict the cell parameters after having them laminated with a certain kind of glass. The answer may be obtained mostly empirically. In this paper we will try to fill this gap by providing experimental tests of various kinds of glass and also describing a measurement procedure and analysing associated uncertainties. Determination of which type of glass is more favourable from a utility point of view is of great importance. However, it represents a considerable metrological challenge to deduce such information from small-scale samples.

2. Experimental

For the test we used five different commercially available types of glass to be potentially applied in PV modules. The glass types differ in thickness, surface structure and optical properties (Tab. 1). No antireflection coating and nanoscale texture was applied as it was confirmed from transmission measurements.

Table 1. Description of examined glass samples.

Sample No.	Thickness [mm]	Type of surface: front / rear
1	3.8	flat / flat
2	3.2	almost flat / delicate random texture
3	4	double side ribbed, 1 mm period
4	3	delicate random texture / moderate texture
5	3.3	delicate random texture / strong texture

We used 30×30 mm silicon solar cells laser-cut from commercial 156×156 mm cells. Attention was paid to select cells with the most homogeneous and similar antireflection coating in order to avoid the influence of an additional factor on the results of experiment. A standard configuration of components was used for the lamination process with a peak temperature of 157°C. The EVA foil of high transmittance was selected on the basis of preliminary tests. Due to the effects of possible dirtiness reported in the literature [10] all the glass samples were placed with the strongly textured side to the EVA foil.

Prior to lamination into mini-modules, the electrical parameters of silicon solar cells were measured using a PET Photo Emission Tech AAA class solar simulator in the Standard Test

Conditions (STC; Irradiance -1000 W/m^2, temp. 25°C). The certified solar cell standard from Fraunhofer ISE was used for the device calibration. Similarly, after the lamination process the mini-modules with different front glass types were measured and characterized again. However, for the electrical characterization after lamination a 32×32 mm mask was used to unify the measurement conditions and to avoid an additional light guiding effect that can be neglected in the case of a standard module. Thanks to initial measurements with the soldered ribbons and measurements of mini-modules containing only one cell we did not introduce other sources of losses, such as an increased resistance and cell mismatch [13]. In order to obtain convincing and converging results the whole experiment from laser cutting to the final measurements after lamination was repeated four times.

The optical characterization of examined samples was performed using UV-VIS-NIR spectroscopy and a procedure accredited by the Polish Centre for Accreditation. The Perkin Elmer Lambda 950S equipped with an integrating sphere and removable attachments was applied to determine the total and diffused components of transmittance and reflectance. We used the certified white diffused spectral reflective standard from Perkin Elmer for the device calibration.

To be convinced that the measured parameters depend only on the properties of glass and no additional damage was introduced during the lamination and measurements we applied the electroluminescence (EL) imaging at the beginning and at the end of the experiment ($I_{FRW} = 0.29$ A $\sim I_{SC}$, $U_{FRW} = 0.6$ V).

3. Results and discussion

In Fig. 1 the morphologies of the examined glass types were presented. The images were taken from the side without or with only a slight texture. For obvious reasons the double-sided flat glass was omitted in this characterization. Additionally, a sketch of each morphology was given as a guide for the eye.

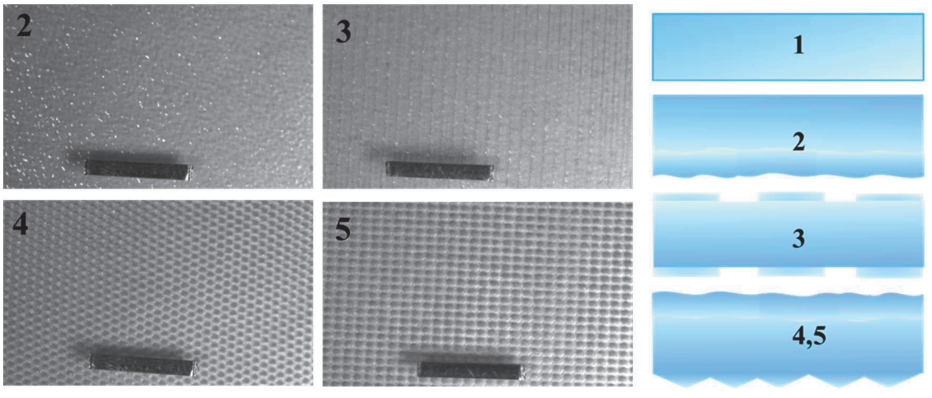

Fig. 1. Optical images of the examined glass types and sketches of their morphologies. A scale bar 1 cm.

The measured total transmittance can be seen in Fig. 2a. The quartz plate (Q), which transmittance is teorethically limited by the Fresnel reflection was used as a reference ($T_{theoretical}$ slighly above 93%). The maximum total transmittance in a visible range exceeded 90% whereas for most of the glass types it oscillated between 88 and 90%. Only the double-sided ribbed glass displayed a clearly noticeable lower transmittance of about 85%. The examined glass types were

slightly different in the UV absorption band, while some of them revealed a slight (sample no. **5**) or moderate (sample no. **1**) absorption in the near-infrared tail caused by the residual ion oxides (inset). No antireflection coating effect was observed for all of the examined samples. On the basis of measured transmittance curves the effective parameter values were calculated taking into account both the theoretical A.M. 1.5 global solar scpectrum [14] and the measured spectrum of solar simulator used for the cell measurements, to check whether they may cause any difference during measurements. These results are summarized in Tab. 2. The reference quartz plate was characterized by the higest effective transmitttance of 92.87%, close to the teoretical value. Among glass types, the highest effective transmittance was obtained for sample no. **2** – 90.75%, and the lowest for sample no. **3** – 85.05%. Except for the clearly outstanding doble-sided ribbed glass sample other glass types had comparable effective transmittance values (differing by less than 2%). It will be valuable to verify how such similar glass types affect the PV performance. A minor difference was found when the measured spectrum of solar simulator was applied to the calculations (up to 0.05%). Additionally, we measured the diffused transmittance component and calculated the haze parameter H as an indicator of the degree of light scattering. The haze parameter is a ratio of diffused and total transmittance values expressed in per cent. In the visible range, it was rather steady; therefore, due to the simplification, a single wavelength was chosen for calculations. The haze of the glass samples was clearly increasing with the degree of texture development. It took values between 1.5 and nearly 70% found for flat and strongly textured glass types, respectively. Another important aspect of mini-module measurements will be revealing whether strong or weak haze directly influences the cell parameteres.

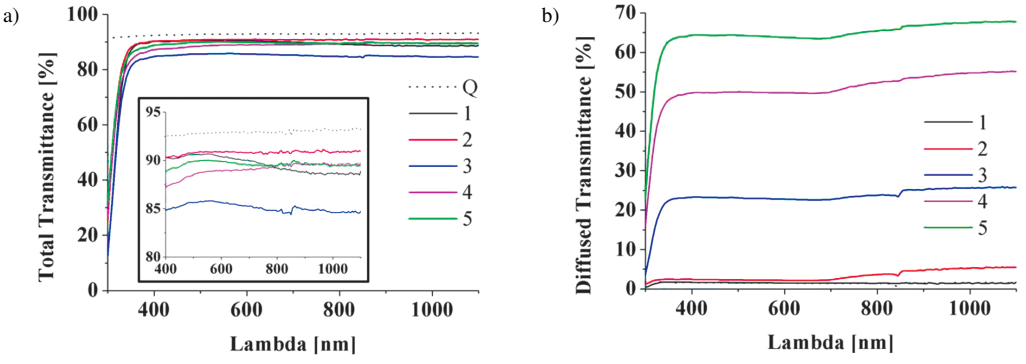

Fig. 2. The measured transmittance values of the glass samples: a) total and b) diffused.

Table 2. The parameter values calculated from optical characterization.

Sample No.	Effective total transmittance [%]		Haze H for 630 nm [%]
	AM 1.5 spectrum	Solar simulator spectrum	
Quartz Q	92.87	92.91	
1	89.62	89.63	1.57
2	90.75	90.79	2.28
3	85.05	85.08	24.28
4	88.95	89.01	53.22
5	89.54	89.57	68.25

Subsequently, the reflectance measurements were performed for bare cells before and after the lamination process. Based on the measurement results of 5 cells the average reflectance and standard deviation were calculated (Fig. 3). The average effective reflectance was 8.94% which varied among samples by ±0.45%, as indicated by the standard deviation. The changes in measurement results reflect inhomogeneity of the samples – variation in thickness of antireflection coating (ARC) or in arrangement of the samples during measurement. The samples' arrangement may result in different amounts of highly reflecting finger contacts in the 0.5×1.5 cm area lit by the measuring beam. In order to recognize such a variation as significant, the uncertainty of the measurements should be discussed. Among the general uncertainty components the ones resulting from the applied calibration standard and spectrophotometer can be omitted since they were the same in all measurements. Hence, the component that matters is the type A uncertainty associated with the measurement accuracy and repeatability. For the used measurement setup it was assessed to be at a level of 0.022%, as the standard deviation from 11 measurements of a standard sample. This confirms that the observed difference describes the actual sample variation. The diffused reflectance values were almost the same as the total one, thus the polycrystalline Si solar cells with typical isotropic texture were recognized as fully scattering surfaces.

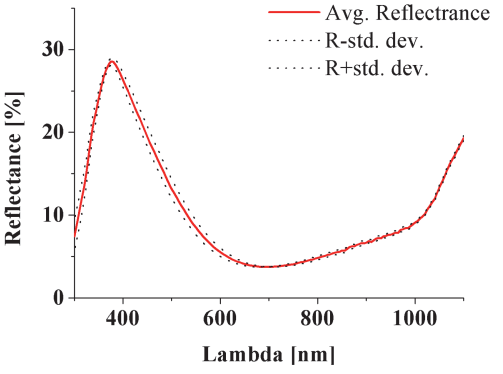

Fig. 3. The average total reflectance of silicon solar cells before lamination.

After lamination the reflectance profile changed significantly (Fig. 4a). In a range from 300 to 380 nm the effect of glass absorption was pronounced. The reflectance maximum around 400 nm unambiguously decreased from about 28.5 nm to around 10% of it or even below. Contrary to this trend, the global minimum around 700 nm slightly increased (∼ 2%). The calculated values of effective reflectance coefficients confirmed the general decrease of reflectance after lamination for each kind of glass (Tab. 3). It should be emphasized that the difference between the average R_{eff} values of other glass samples was in the order of variation of the samples before lamination. However, this time the standard deviation of all series was considerably smaller and enabled to treat those values as significant. Additionally, the influence of the highly reflective contacts was lower, since the beams reflected from the scattering contacts at higher angles were trapped due to the total internal reflection effect. Analysis of the diffused reflectance component of the samples after lamination indicated its significantly reduced share, compared with the solar cells before lamination (Fig. 4b). Moreover, some kind of averaging was observed despite the clear difference in haziness of examined glass samples. The double-sided flat glass revealed a 26.7% share of the diffused component, while samples with delicate, moderate and strong texture (analogically haziness) had 31.9, 31.8 and 37.3% shares, respectively (Tab. 3). This behaviour can be attributed to the glass surface roughness reduced by covering it with EVA foil. The kind of

effective medium between the glass inner roughness and EVA foil was created providing a much smoother transition of the refractive index than for the previous glass/air interface. In such a case a share of the diffused component is determined by the scattering properties of the solar cell and roughness of the glass front surface. The double-sided ribbed glass (**3**) with non-compensated macro texture on the front side resulted in the highest share of diffused components – 46.1%.

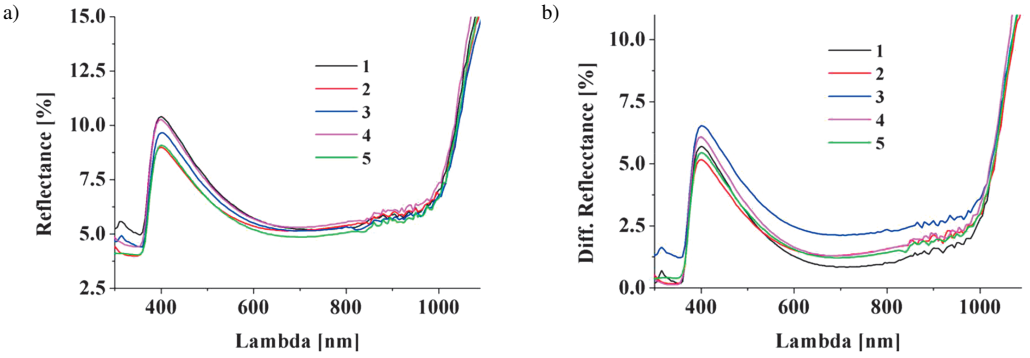

Fig. 4. The total and diffused components of reflectance from laminated mini-modules from a selected series.

Table 3. The effective reflectance after lamination, share of diffuse reflectance component and change of I_{SC} after lamination – averaged for all series.

Sample No.	Avg. R_{eff} after lamination [%]	R_{dif} after lamination [%]	ΔI_{SC} after lamination [%]
1	7.26 ± 0.41	26.7	-2.64 ± 0.99
2	6.77 ± 0.2	31.9	-0.51 ± 0.46
3	6.68 ± 0.09	46.1	-3.47 ± 0.61
4	7.04 ± 0.12	31.8	-1.22 ± 0.70
5	6.67 ± 0.26	37.3	-1.46 ± 0.27

Optical characterization provided important information on the components used for lamination as well as on the complete mini-modules. However, the most important outcome in this case was obtained from analysis of electrical parameters of the cells in respect to the initial state before lamination. A critical parameter was the change of short-circuit current since it is directly proportional to the number of incident photons resulting from the optical match of the whole laminated systems. Despite the reduction in R_{eff} after lamination for all the samples, a slight drop of I_{SC} was observed and it will be discussed in the following Section. Additionally, an increase of V_{OC} – on average 8.6 mV (1.34%) – was noticed. This may be due to the higher heat capacitance resulting in the slower cell heating during flash light measurements of laminated mini-modules. It probably will not concern the actual, outdoor operating modules since there will be enough time to reach higher temperature. Nevertheless, a different surface structure of the glass may influence the modules' cooling rate and affect their operation voltage.

The average short-circuit current I_{SC} drop was between ~ 0.5 and 3.5% for different glass types and the standard deviation calculated from all four series was between 0.27 and 1% (Tab. 3). The necessary uncertainty budget was estimated and its components were as following: 1) since the uncertainty of the calibration cell and measuring device refer to absolute values only they were omitted in these comparative studies; 2) the type A uncertainty of a statistical distribution

was assessed to be 0.2%; 3) the temperature variation; since it was controlled with an accuracy of 1°C, the standard thermal coefficient for a silicon solar cell was used (0.05%) [15]; 4) the instability of the solar simulator lamp and its calibration uncertainty determined from the calibration standard measurements (0.275%) were the major sources of uncertainty. The total uncertainty was calculated from the square root of the sum of squared components. It was assessed to be at a level of $\sim 0.7\%$ of I_{SC} for $k = 2$ and it explained to a large extent the observed scattering of results.The remaining part can be attributed to other experimental sources of uncertainty, i.e. the samples' cleaning, stacking, lamination and arrangement during measurements etc., but they are difficult to be properly estimated.

The double-sided flat glass (sample no. **1**) considered in this experiment was found rather inappropriate, resulting in a 2.64% decrease of I_{SC}. Most probably, no additional light trapping mechanism and absorption in the glass deduced from transmittance measurements (Fig. 2) were responsible for the observed results. The best glass – giving only a 0.5% drop – was that of sample no. **2** with a very fine front texture and a delicate texture on the rear, additionally characterised by the highest transmittance. An approximately 0.5% decrease of I_{SC} after lamination was also reported by other researchers [13].

Comparable results were obtained for the glass types with a delicate front texture and a well-developed rear one (samples no. **4** and **5**). A drop was of the order of 1.2–1.5%. Taking into account the uncertainty and scattering of the results it is difficult to judge whether this is caused by the texture development or haziness. However, this effect was clearly seen for the ribbed glass. In this case a drop of I_{SC} was the highest, reaching about 3.5%. In this way the high haziness and light trapping were not confirmed for the macroscale ribbed glass. This kind of glass may be beneficial in the case of lower operating temperature resulting from faster cooling but it requires further careful studies.

In Fig. 5 the average I_{SC} drop is correlated with the average effective reflectance after lamination. Considering samples no. **1** and **2** it can be found that some correlation between the reflectance and I_{SC} drop is noticeable for low-hazy glass types, while it is hardly observable for other samples. For example, for the double-sided ribbed glass the reflectance was one of the lowest but the I_{SC} drop was the highest. Additionally, comparison of samples no. **1** and **2** provided the evidence that glass transmittance may not be sufficient to predict the cell performance after lamination. The difference in effective transmittance was $\sim 1.1\%$, whereas the difference in I_{SC} drop was $\sim 2.1\%$. On the other hand, the level of transmittance may provide a valuable first conjecture as it follows from comparison of samples no. **2** and **5**. The difference in effective transmittance was $\sim 1.21\%$ and the difference in I_{SC} drop was $\sim 1.45\%$. These two examples confirm the necessity of experimental verification of the components used for the lamination.

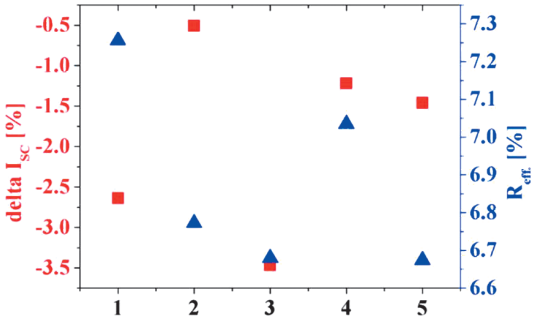

Fig. 5. Compilation of results for ΔI_{SC} and R_{eff} after lamination.

Finally, electroluminescence images of the samples before and after tests shown in Fig. 6 confirm that the observed results were not caused by any internal damages. If there is any cell breakage or contact discontinuity, it results in clearly visible darkening of the defective area. The darkened area seen in the EL images repeated in both pictures reflects dislocation and initial wafer non-idealities. No traces of damage were found for all the samples of other series.

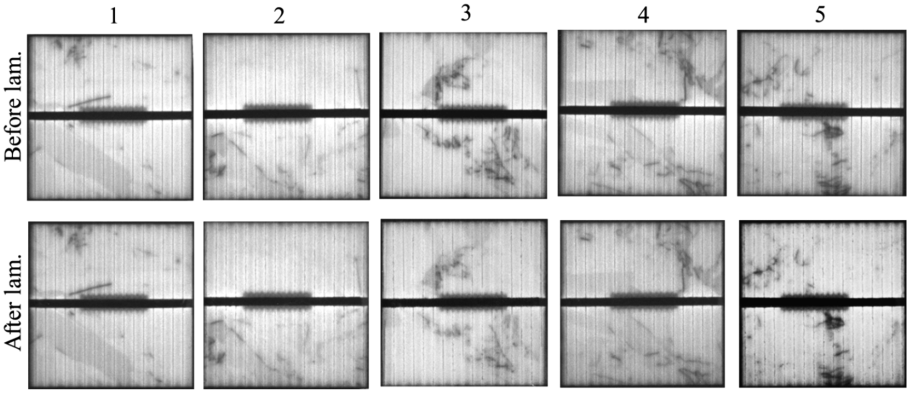

Fig. 6. Electroluminescence images of selected series of cells before and after the lamination process. The cells' size was 30×30 mm.

4. Summary and conclusions

The optical properties and performance of photovoltaic modules were examined for various glass samples additionally characterized by differently developed surfaces. This examination confirmed the necessary experimental character of the photovoltaic glass evaluation. For that purpose a complex procedure was developed including optical and electrical measurements as well as samples' control. The accuracy of evaluation was assessed by determination of the distribution of scattering and components of uncertainty. It was shown that for the examined glass samples I_{SC} of photovoltaic modules can drop from 0.5 to 3.5%, what confirms the necessity of appropriate glass selection. Among the examined glass types the best performance was obtained for the sample with a high initial transmittance, low reflectance after lamination and rather low haziness resulted from its delicate texture.

Acknowledgements

The authors gratefully acknowledge the financial support from The National Centre for Research and Development and The National Fund for Environmental Protection and Water Management within the scope of the project: "Innovative flexible photovoltaic cover", No. GEKON2/O4/268473/23/2016.

References

[1] Snapshot of Global Photovoltaic Markets. (2016). IEA International Energy Agency PVPS. *www.iea-pvps.org/fileadmin/dam/public/report/statistics/IEA-PVPS_-_A_Snapshot_of_Global_PV_-_1992-2016__1_.pdf.*

[2] Photonovltaic Raport. (2017). Fraunhofer ISE: *www.ise.fraunhofer.de/content/dam/ise/de/documents/publications/studies/Photovoltaics-Report.pdf.*

[3] Czanderna, A.W., Pern, F.J. (1996). Encapsulation of PV modules using ethylene vinyl acetate copolymer as a pottant: A critical review. *Solar Energy Materials and Solar Cells*, 43(2) 101–181.

[4] El Amrani, A., Mahrane, A., Moussa, F.Y., Boukennous, Y. (2007). Solar Module Fabrication. *International Journal of Photoenergy*, ID 27610.

[5] Lange, R.F.M., Luo, Y., Polo, R., Zahnd, J. (2011). The lamination of (multi)crystalline and thin film based photovoltaic modules. *Progress in Photovoltaics Research and Applications*, 19(2), 127–133.

[6] Drabczyk K., Panek P. (2012). A comparative study of EVA with and without thermal history for different lamination process parameters. *Materials Science and Engineering B-Advanced Functional Solid State Materials*, 177(15), 1378–1383.

[7] Mansur, A.A.P., Nascimento, O.L., Vasconcelos, W.L., Mansur, H.S. (2008). Chemical functionalization of ceramic tile surfaces by silane coupling agents: polymer modified mortar adhesion mechanism implications. *Materials Research*, 11(3), 293–302.

[8] Chen, L., Wang, Q., Chen, W., Huang, K., Shen, X., (2016). Investigation of a novel frosted glass with regular pit array texture. *Journal of Materials Processing Technology*, 238, 195–201.

[9] Son, J., Kundu, S., Verma, L.K., Sakhuja, M., Danner, A.J., Bhatia, C.S., Yang, H. (2012). A practical superhydrophilic self cleaning and antireflective surface for outdoor photovoltaic applications. *Solar Energy Materials & Solar Cells*, 98, 46–51.

[10] Said, S.A.M., Al-Aqeeli, N., Walwil, H.M. (2015). The potential of using textured and anti-reflective coated glasses in minimizing dust fouling. *Solar Energy*, 113, 295–302.

[11] Ballif, C., Dicker, J., Borchert, D., Hofmann (2004). Solar glass with industrial porous SiO2 antireflection coating: measurements of photovoltaic module properties improvement and modeling of yearly energy yield gain. *Solar Energy Materials & Solar Cells*, 82, 331–344.

[12] Wohlgemuth, J., Cunningham, D., Shaner, J., Nguyen, A., Ransome, S., Artigao, A. (2005). Crystalline Silicon Photovoltaic modules with anti-reflective coated glass. *Photovoltaic Specialists Conference, Conference Record of the Thirty-first IEEE*, 1015–1018.

[13] Yang, H., Wang, H., Cao, D., Sun, D., Ju, X. (2015). Analysis of Power Loss for Crystalline Silicon Solar Module during the Course of Encapsulation. *International Journal of Photoenergy*, ID 251615, *http://dx.doi.org/10.1155/2015/251615.*

[14] Reference Solar Spectral Irradiance. Air Mass 1.5, American Society for Testing and Materials (ASTM). *Terrestrial Reference Spectra for Photovoltaic Performance Evaluation, http://rredc.nrel.gov/solar/ spectra/am1.5/*

[15] Ponce-Alcántara, S., Connolly, J.P., Sánchez, G., Míguez, J.M., Hoffmann, V., Ordás, R. (2014). A statistical analysis of the temperature coefficients of industrial silicon solar cells. *Energy Procedia,* 55, 578–588.